

# Investigating Electrical and Ferroelectric Properties of Nd Doped BiFeO<sub>3</sub>-PbTiO<sub>3</sub> Solid Solutions

Ram Chhavi Sharma<sup>1\*</sup>, Manoj Baloni<sup>2</sup>, Hemant Singh<sup>3</sup>

\*Corresponding Author Email: [rcsharma@sgtuniversity.org](mailto:rcsharma@sgtuniversity.org)

<sup>1\*</sup>Department of Physics, Faculty of Applied and Basic Sciences, SGT University, Gurugram(Haryana) -122505, India.

<sup>2</sup>Department of Physics, SGRR(PG) College Dehradun, Dehradun, Uttarakhand, India.

<sup>3</sup>Department of Physics, Sri Dev Suman Uttarakhand University, Badshahithol, Tehri Garhwal, Pt. L. M. S. Campus, Rishikesh, Uttarakhand, India.

**Abstract:** The effect of different Nd and PT compositions on the electrical and ferroelectric properties of (1-y)Bi<sub>1-x</sub>Nd<sub>x</sub>FeO<sub>3</sub>-yPbTiO<sub>3</sub> solid solutions, where x = 0.05, 0.10, 0.15, 0.20 and y = 0.1, 0.2, 0.3, and 0.4, was investigated to optimise material performance. Nd doping enhances the frequency-dependent dielectric properties of produced solid solutions. However, an anomaly in the dielectric loss tangent, which is consistent with the Debye relaxation process, is observed for compositions with x<0.10 and y≥0.2 values in the frequency range of 1 KHz to 1 MHz. Dielectric anomalies were more noticeable around the transition temperature in temperature-dependent dielectric characteristics plots, suggesting stronger magnetoelectric interactions. The decrease in the dielectric constant for solid solution compositions with y ≥0.3 indicates the presence of MPB with BFO due to an increase in the tetragonal phase of the PbTiO<sub>3</sub> compound. As Nd content increases, temperature-dependent dielectric permittivity predicts relaxor-type ferroelectric performance for y=0.4 composition of solid solutions. A ferroelectric investigation showed that saturation polarisation, remnant polarisation, and coercive field of all prepared solid solutions decrease with increased Nd doping. However, for y>0.3 composition, a substantial rise in these parameters was observed, which is a result of electric order dominating over magnetic order in solid solutions. The study reveals that Nd doping reduces leakage current, making it a promising contender for future applications

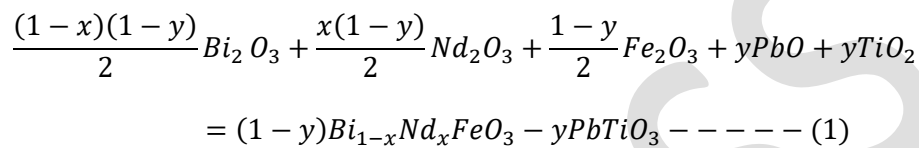
**Keywords:** *Solid solution, Nd doping, Electrical, Ferroelectric, remnant polarisation.*

## 1. INTRODUCTION

Relaxor ferroelectrics with low remnant polarisation ( $P_r$ ) and moderately high saturated polarisation ( $P_{max}$ ) have garnered significant interest in energy storage applications [1]. The substitution of ions or creating solid solutions with alternative materials can produce the relaxor ferroelectric phase. Due to excellent saturation polarisation, studies of the  $\text{BiFeO}_3\text{-BaTiO}_3$  (BF-BT) solid solution demonstrate that including relaxor dielectric components can successfully modify the energy storage outcomes. However, high  $P_r$  values limit pure BFO-BT's energy storage values [2]. Due to remarkable maximum polarisation ( $P_{max} > 100 \mu\text{C}/\text{cm}^2$ ),  $\text{BiFeO}_3$  (BFO) was found to be a promising lead-free energy storage material with the potential for excellent energy storage performance [3]. With a deformed rhombohedral perovskite structure and  $R3c$  space group symmetry, BFO possesses both G-type anti-ferromagnetism and ferroelectricity, with matching Curie temperatures of 1103K and Neel temperatures of 643 K [4]. The ferroelectricity results from the movement of  $\text{Bi}^{+3}$  ions from centrally symmetric locations about the surrounding oxygen ions. BFO has many fascinating features but disadvantages, such as weak magnetisation, high leakage current, high dielectric loss, low ferroelectric reliability, secondary phase production, and weak magnetoelectric coupling. Perovskite-type composites, like  $\text{PbTiO}_3$  or  $\text{BaTiO}_3$ , enhance BFO's multiferroics properties and energy storage capabilities. Because of its high polarisation and dielectric constant, ferroelectric material  $\text{PbTiO}_3$  (PT) is used in this work. It settles the composite's perovskite phase and, because of the differences in crystal symmetry between PT and BFO, also generates a morphotropic phase boundary (MPB) with BFO. To lower leakage current and enhance the functional characteristics of BFO, we created a BFO-PT solid solution. Additionally, doping it with rare earth elements improved BFO's multiferroics and dielectric characteristics. In the present research, we explore solid solutions' dielectric and ferroelectric features and study their electrical and ferroelectric properties with varying Nd and PT compositions. In addition, we examine the relaxor behaviour of solid solution for an appropriate Nd and PT composition, which reveals the effectiveness of the energy storage system.

## 2. EXPERIMENTAL PROCEDURES

Solid solutions of  $(1-y)\text{Bi}_{1-x}\text{Nd}_x\text{FeO}_3-y\text{PbTiO}_3$  with  $x$  varying from 0.05 to 0.20 in increments of 0.05 and  $y$  ranging from 0.1 to 0.4, were synthesised using the solid-state reaction technique. Analytical-grade reagent powders ( $\text{Bi}_2\text{O}_3$ ,  $\text{Fe}_2\text{O}_3$ ,  $\text{PbO}$ ,  $\text{Nd}_2\text{O}_3$ , and  $\text{TiO}_2$ ) were accurately weighed and thoroughly mixed in acetone for four hours using an agate mortar. There were no deviations in the proportions taken. The following equation represents the reaction.



We calcined the finely ground powders in a furnace for two hours at 800, 810, 830, and 840 degrees Celsius for different  $\text{PbTiO}_3$  composition compositions. A 5% excess of  $\text{Bi}_2\text{O}_3$  was added to the starting reactants during the synthesis process to prevent the formation of secondary phases of  $\text{Bi}_2\text{Fe}_4\text{O}_9$ . After adding several drops of a concentrated fluid polyvinyl alcohol (PVA) binder (5%), we processed each powder composition for an additional two hours in the agate mortar. Pellet specimens, with a diameter of 6 mm and a thickness of 1 mm, were created by compressing mixed powders of different compositions into circular discs while imposing pressure of  $1.5 \times 10^9$  Pascal's and then heated the discs to 820, 830, 850, and 860 degrees Celsius for two hours. Using an X-ray diffraction technique at room temperature on a Bruker D8 Advance X-ray diffractometer with  $\text{CuK}$  radiation at a wavelength of 1.5406 Å, the samples' crystal structure and phase evolution were investigated [5]. The surface morphology of artificial samples was analysed using Carl Zeiss EVO18 scanning electron microscopes with an electron beam intensity of 20 Kev. We used an argon laser with a wavelength of 514.5 nm as the stimulation source for the Renishaw micro Raman microscope to conduct the Raman spectroscopy investigations. Sharma et al. 2024 provide comprehensive information on solid solutions' structural and average crystalline size determination [6]. We performed dielectric measurements in the temperature range of 35°C to 400°C, with 5°C phase increments, using a computer-controlled Alpha-A High Impedance Analyzer (Novo Control) within a frequency bandwidth of  $10^2$  Hz to  $10^6$  Hz. and also

investigated the solid solutions' P-E loops and leakage current versus voltage characteristics using a Radiant Precision Multiferroic Tester operating at 10 Hz.

### 3. RESULTS AND DISCUSSION

#### 3.1 Dielectric Analysis of Nd-doped BiFeO<sub>3</sub>-PbTiO<sub>3</sub> Solid Solution with Frequency at Ambient Temperature

Figure 1 to 4 illustrates the variability of the dielectric constant and dielectric loss tangent ( $\tan\delta$ ) of  $(1-y)1-x\text{Nd}_x\text{FeO}_3-y\text{PbTiO}_3$  solid solutions in the frequency range of 100Hz to 1MHz for various  $x$  and  $y$  compositions at ambient temperature. We discovered that the dielectric constant is noticeably large at low frequencies and progressively drops as the applied alternating field frequency rises for all prepared solid solutions with varying  $x$  and  $y$  compositions. We used the interfacial space charge relaxation process to explain the variation in the dielectric constant [7,8]. Bismuth ( $\text{Bi}^{+3}$ ) and oxygen ( $\text{O}^{-2}$ ) vacancies on the composition's A-site produce space charges at low frequencies. Applied electric field, and these space charges are in phase, which aids in preserving the dielectric constant. Additionally, the production of  $\text{O}^{-2}$  -vacancies brought on by the vaporescent nature of the  $\text{Bi}^{+3}$  and the transformation from  $\text{Fe}^{+3}$  to  $\text{Fe}^{+2}$  causes the dielectric constant to increase with an increase in Nd doping of all solid solutions with varied  $y$  compositions [9]. The dielectric constant value decreases in solid solutions for  $y \geq 0.3$  compositions, or the amount of  $\text{PbTiO}_3$  increases, which is mainly due to  $\text{PbTiO}_3$ 's dominance of tetragonality, which settles the composite's perovskite phase and creates an MPB with BFO due to the crystal symmetry differences between PT and BFO [10,11,12].

The dielectric losses, determined by the energy lost by the device, are further amplified by space charge polarisation and domain wall resonance. For all of the created solid solutions with different  $x$  and  $y$  components, we found that the dielectric loss tangent decreases with increasing frequency and dielectric loss is high near the grain boundary at low frequencies due to energy dissipation caused by amalgamated space charge polarisation and low at high frequencies due to domain wall motion suppression.

Additionally, as the frequency of the applied electric field increases, the redirection of the space charge slows down and eventually stops. For compositions with  $x < 0.10$  and  $y \geq 0.2$ , in the 1 KHz–1 MHz frequency range, the dielectric loss tangent exhibits anomaly; this is compatible with the Debye relaxation process [13]. Similar outcomes have been observed with rare earth-doped multiferroic composites [14]. The samples are helpful for capacitor, transducer, and microwave applications due to their high dielectric constant and low loss.

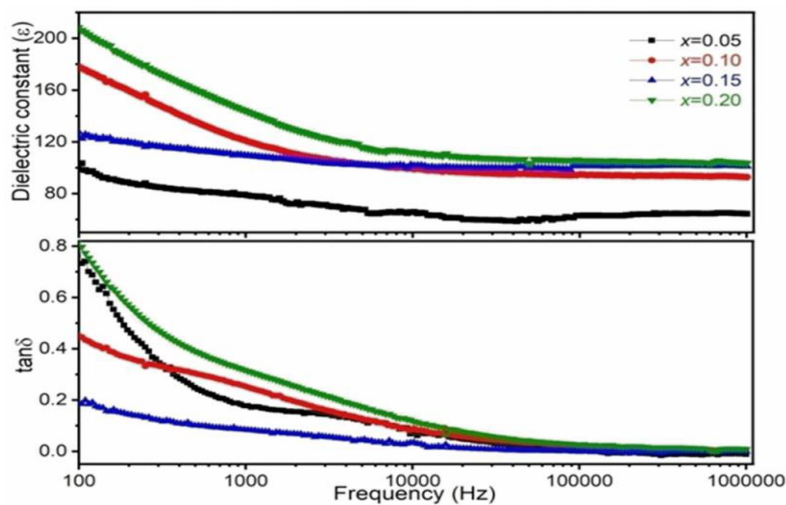


**Fig. 1** Frequency dependence of  $\epsilon$  and  $\tan\delta$  for  $(1-y)\text{Bi}_{1-x}\text{Nd}_x\text{FeO}_{3-y}\text{PbTiO}_3$  solid solutions with  $y=0.1$  and different  $x$  compositions.

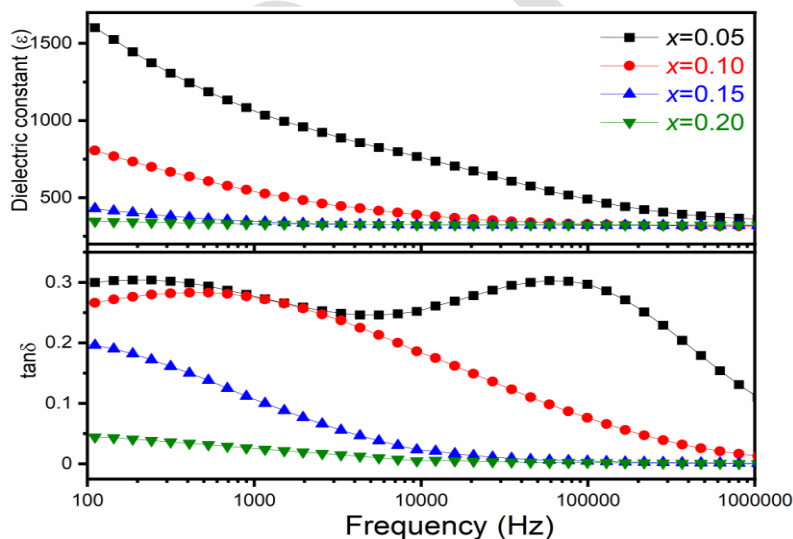


**Fig. 2** Frequency dependence of  $\epsilon$  and  $\tan\delta$  for  $(1-y)\text{Bi}_{1-x}\text{Nd}_x\text{FeO}_{3-y}\text{PbTiO}_3$  solid solutions with  $y=0.2$  and different  $x$  compositions.

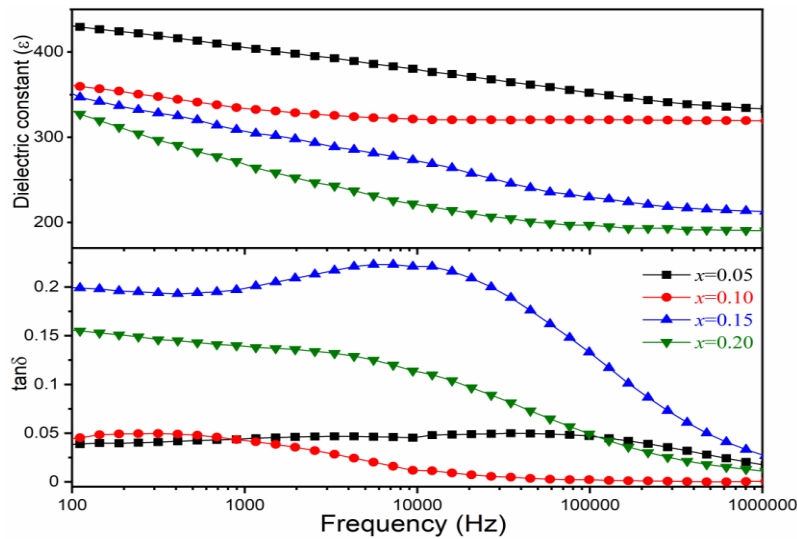


**Fig. 3** Frequency dependence of  $\epsilon$  and  $\tan\delta$  for  $(1-y)\text{Bi}_{1-x}\text{Nd}_x\text{FeO}_{3-y}\text{PbTiO}_3$  solid solutions with  $y=0.3$  and different  $x$  compositions.

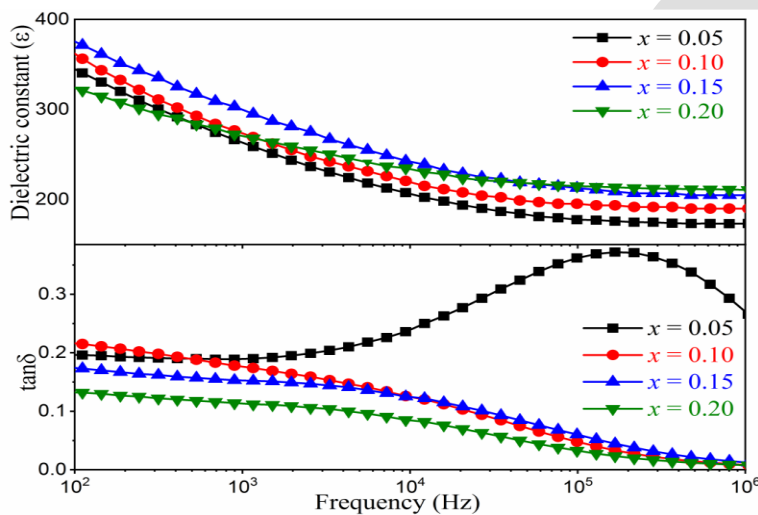


**Fig. 4** Frequency dependence of  $\epsilon$  and  $\tan\delta$  for  $(1-y)\text{Bi}_{1-x}\text{Nd}_x\text{FeO}_{3-y}\text{PbTiO}_3$  solid solutions with  $y=0.4$  and different  $x$  compositions.

### 3.2 Dielectric Analysis of Nd Doped $\text{BiFeO}_3\text{-PbTiO}_3$ Solid Solution with Temperature

Figure 5 to 8 illustrates the variability of the dielectric constant and dielectric loss tangent ( $\tan\delta$ ) of  $(1-y)\text{Bi}_{1-x}\text{Nd}_x\text{FeO}_{3-y}\text{PbTiO}_3$  solid solutions with temperature in the frequency range of 1kHz to 1MHz for various  $x$  and  $y$  compositions. As the temperature rises, the relative dielectric constant steadily rises, mildly extending into the region of high temperature, which is a characteristic feature of ferroelectric materials. Dielectric anomalies, however, are seen at all frequencies as the  $x$  and  $y$  content rises. The coexistence of two structure phases distinguishes all solid solutions for  $y \geq 0.2$  compositions.

According to earlier reports [15,16], rare-earth substitution lowers the Curie Temperature  $T_c$  in the BFO perovskite solid solutions. The diminished repulsive impact of short-range against ferroelectric ordering reduces the transition temperature by adding Nd content. Furthermore, the powerful interaction among the  $\text{Bi}^{3+}/\text{Pb}^{2+}$ (A site) and  $\text{Ti}^{4+}/\text{Fe}^{3+}$ (B-site) cations is responsible for the high transition temperature and high tetragonal strain in solid solutions with  $y \geq 0.2$  compositions. The  $\text{Nd}^{3+}$  substitution decreases the coupling between the cations and reduces the tetragonal strain in solid solutions. Further, we observed that dielectric arrangement improves as the Nd level increases.

The charge carriers generated by defects and thermal action cause the dielectric loss tangent to be high at higher temperatures and low at lower ones. The reason is that as the temperature rises, charge carriers gain energy and dielectric loss increases. The detected anomalies at transition temperature in the dielectric loss for all solid solutions with various x and y components are due to the diminishing magnetic order on electric order in a magneto-electrically structured system (Landau-Devonshire phase transition theory). For all prepared samples, we found that the dielectric loss tangent reduces with increasing  $\text{Nd}^{3+}$  ions doping, indicating enhanced stability, sample resistivity and charge carrier movement. The increase in  $\tan \delta$  value in high-temperature regions indicates that sample conductivity increases. Furthermore, the motility of charge carriers increases with temperature, which improves polarisation, resulting in high dielectric losses and accumulation of charges at grain boundaries [17].

The effectiveness of oxygen vacancies and polarisation at high temperatures also explain the rise in  $\tan \delta$ . The calcination and sintering processes generate electrons and oxygen vacancies. The increase in ionic conductivity at higher temperatures results from these oxygen vacancies, which are not restricted to the unit cell but can affect the entire system [18], which could most likely cause unusual saturation at high temperatures. Auromun et al. [19] also obtained this kind of result. Furthermore, for all produced samples, dielectric loss decreases as doping increases. Also, the peak widens, intensifies, and shifts to the higher temperature region with an increase in frequency, suggesting the presence of a phase transition of diffuse type. Consequently, the temperature-dependent feature of dielectric permittivity reveals the usual attribute of relaxor ferroelectrics, which may be due to the simultaneous substitution of  $\text{Nd}^{3+}$  and  $\text{Pb}^{2+}$  ions for the  $\text{Bi}^{3+}$  site cation and  $\text{Ti}^{4+}$  ion for the  $\text{Fe}^{3+}$  site cation having different Pauling's

electro-negativities and ionic radii. [20]. As a result, these parameters promote ferroelectric relaxor behaviour as these prohibit the long-range structuring of the lattice.

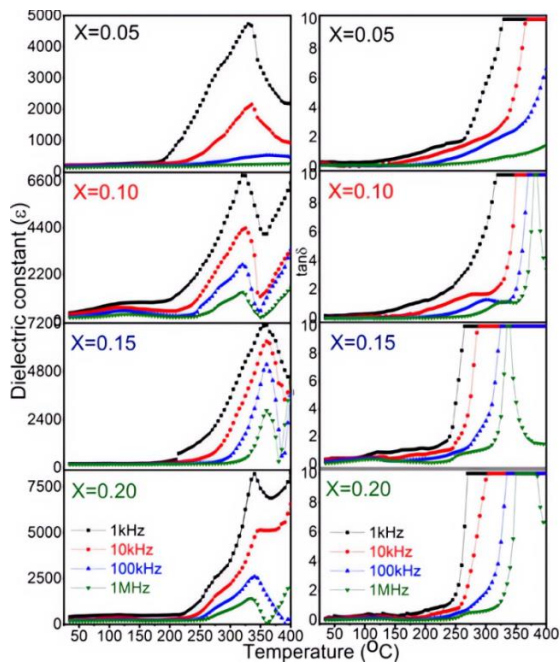


**Fig. 5** Temperature dependence of  $\epsilon$  and  $\tan\delta$  for  $(1-y)\text{Bi}_{1-x}\text{Nd}_x\text{FeO}_{3-y}\text{PbTiO}_3$  solid solutions with  $y=0.1$  and different  $x$  compositions in 1kHz- 1MHz frequency range.

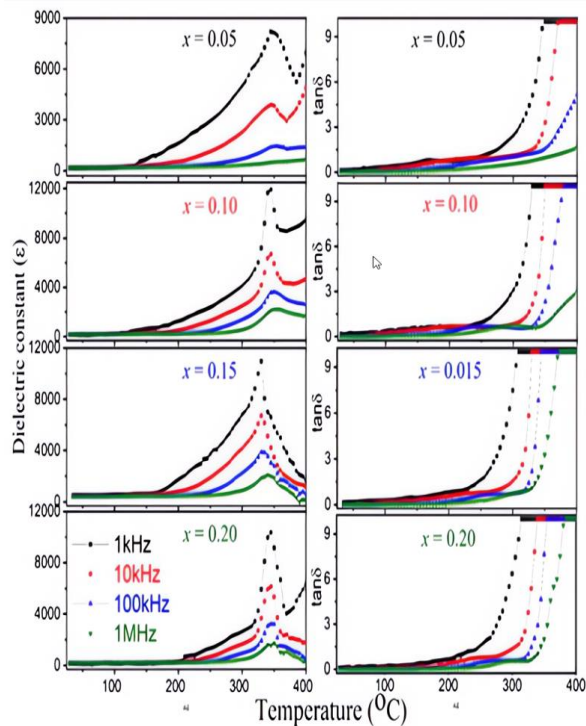


**Fig. 6** Temperature dependence of  $\epsilon$  and  $\tan\delta$  for  $(1-y)\text{Bi}_{1-x}\text{Nd}_x\text{FeO}_{3-y}\text{PbTiO}_3$  solid solutions with  $y=0.2$  and different  $x$  compositions in 1kHz- 1MHz frequency range.



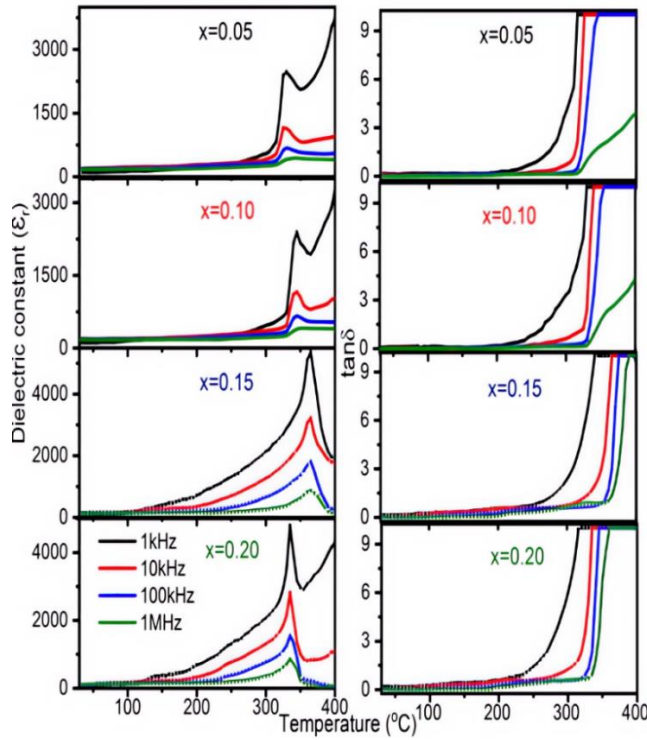


**Fig. 7** Temperature dependence of  $\epsilon'$  and  $\tan\delta$  for  $(1-y)\text{Bi}_{1-x}\text{Nd}_x\text{FeO}_{3-y}\text{PbTiO}_3$  solid solutions with  $y=0.3$  and different  $x$  compositions in 1kHz- 1MHz frequency range.

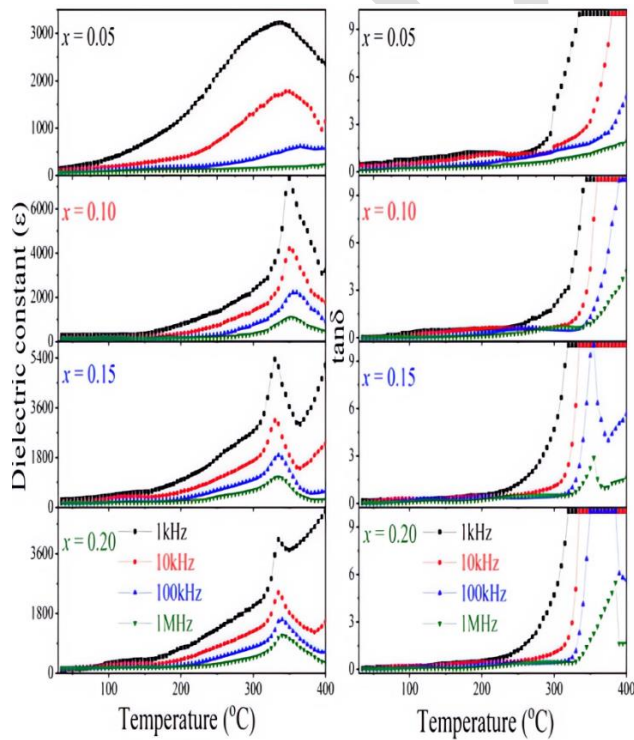


**Fig. 8** Temperature dependence of  $\epsilon$  and  $\tan\delta$  for  $(1-y)\text{Bi}_{1-x}\text{Nd}_x\text{FeO}_{3-y}\text{PbTiO}_3$  solid solutions with  $y=0.4$  and different  $x$  compositions in 1kHz- 1MHz frequency range.

### 3.3 Ferroelectric Properties

The current study determines solid solutions' P-E loops and leakage current vs voltage characteristics using a Radiant precision multiferroics tester at 10Hz frequency. Figures 9 to 12 depict the ferroelectric hysteresis loops of  $(1-y)\text{Bi}_{1-x}\text{Nd}_x\text{FeO}_3\text{-yPbTiO}_3$  solid solutions with different  $x$  and  $y$  compositions at room temperature. The conductive performance of  $\text{BiFeO}_3$  limits its ferroelectric behaviour, which is caused mainly by a larger leakage current. Due to rare earth ions, the rare-earth-doped  $\text{BiFeO}_3\text{-PbTiO}_3$  systems exhibit less conductivity than binary  $\text{BiFeO}_3\text{-PbTiO}_3$  systems [21]. In the prepared samples, ferroelectricity arises from the hybridisation between the O(2p) orbital of the  $\text{BiFeO}_3$  crystal and the Bi ( $6s^2$ ) lone pair, as well as between the Ti(3d) orbital and the O(2p) orbital associated with the ferroelectric distortion in  $\text{PbTiO}_3$ .

Furthermore, for  $y \geq 0.2$  compositions of solid solutions, the simultaneous occurrence of the rhombohedral phase of BFO and the tetragonal phase of PT also contributes to ferroelectricity. It is observed that the saturation polarisation and remnant polarisation of solid solutions are higher for  $x=0.05$  Nd composition and a chosen value of  $y$  composition and then decrease with increasing Nd concentration. The structural distortions and differences in  $\text{Nd}^{+3}$  and  $\text{Fe}^{+3}$  ionic radii may cause a diminution in remnant polarisation. Sahu et al. published a comparable decrease in remnant polarisation in compounds of  $\text{BiFeO}_3\text{-PbTiO}_3$  doped with Sm [22].

Furthermore, theoretical and empirical investigations have shown that the remnant polarisation in materials is affected by oxygen vacancies [23,24]. The high-temperature sintering process produces lead and oxygen vacancies primarily due to PbO evaporation. These vacancies produce defect dipoles with Pb ions. These dipoles produce a polarisation vector, which tends to cause the dipoles to become disoriented [25]. The induced polarisation vector produced by these dipoles needs some additional energy to align in the direction of the field, and the restoring force established as a result of the continuous polarisation helps the domains regain the original state, resulting in a drop in remnant polarisation. In Sr-modified  $\text{BiFeO}_3\text{-PbTiO}_3$  ceramics, Kumar N et al. have observed similar correlations between remnant polarisation and oxygen vacancies [26].

The nature of P-E hysteresis loops in BiFeO<sub>3</sub>-PbTiO<sub>3</sub> solid solutions strongly depends on the delicate balance of Nd and PbTiO<sub>3</sub> compositions. Achieving optimal doping reduces leakage currents and enhances ferroelectric properties, while excessive doping introduces defects and disrupts ferroelectric behaviour. In the present study, all the hysteresis loops in (1-y)Bi<sub>1-x</sub>Nd<sub>x</sub>FeO<sub>3</sub>-yPbTiO<sub>3</sub> solid solutions with varied y compositions become saturated with increasing x composition or Nd doping. As a result, the P-E loops exhibit a pinning effect. According to the defect symmetry principle, oxygen vacancy significantly contributes to the pinning effect in ferroelectrics [27,28]. The values of remnant polarisation and coercive field are reduced in all the samples under investigation with the increase in Nd doping, as indicated in Table 1- 3. The value of remnant polarisation and saturation polarisation, however, increases for y>0.3 composition due to the ferroelectric nature of PbTiO<sub>3</sub> and the fact that electric order predominates over magnetic order in solid solutions.

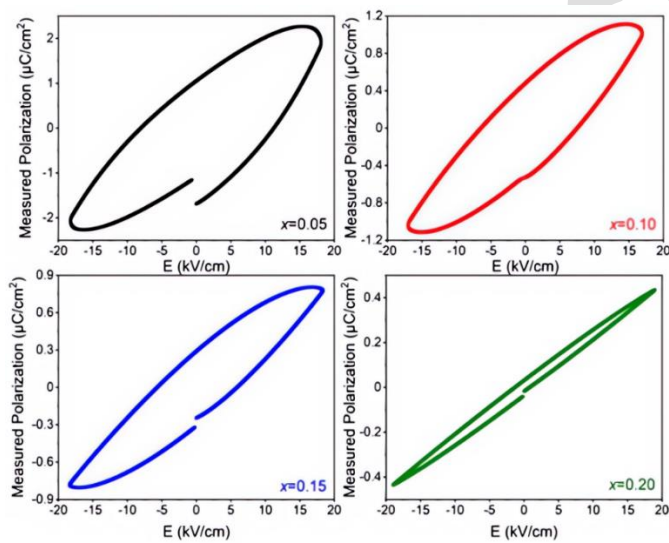


**Fig. 9** P-E hysteresis loops of (1-y)Bi<sub>1-x</sub>Nd<sub>x</sub>FeO<sub>3</sub>-yPbTiO<sub>3</sub> solid solutions with y=0.1 and different x compositions.

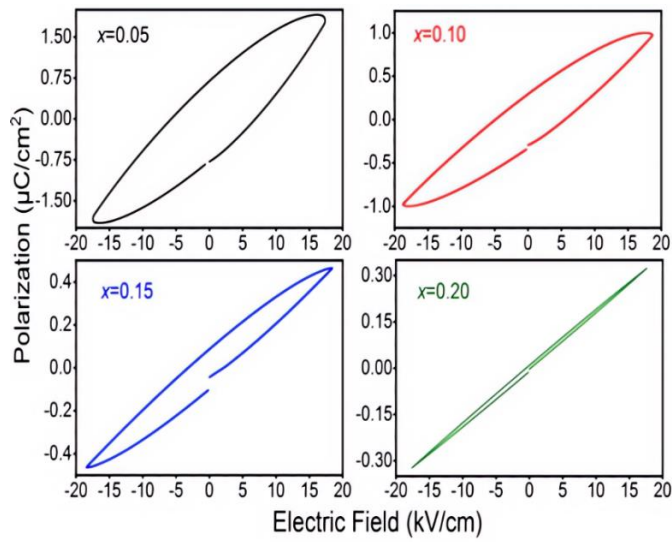


**Fig. 10** P-E hysteresis loops of  $(1-y)\text{Bi}_{1-x}\text{Nd}_x\text{FeO}_{3-y}\text{PbTiO}_3$  solid solutions with  $y=0.2$  and different  $x$  compositions.

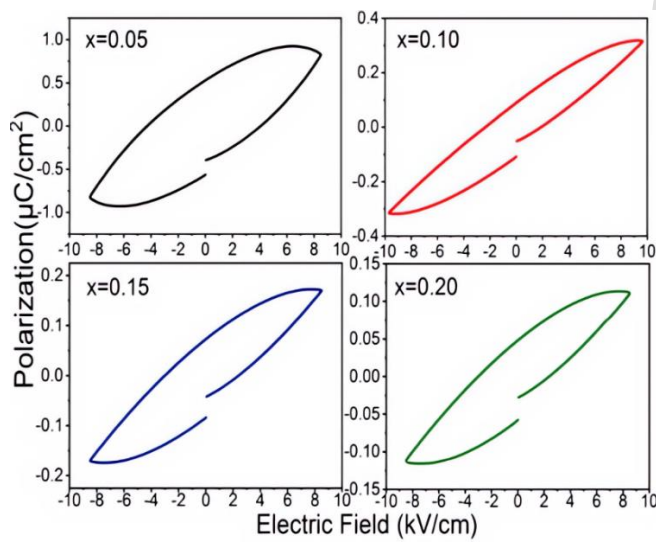


**Fig. 11** P-E hysteresis loops of  $(1-y)\text{Bi}_{1-x}\text{Nd}_x\text{FeO}_{3-y}\text{PbTiO}_3$  solid solutions with  $y=0.3$  and different  $x$  compositions.

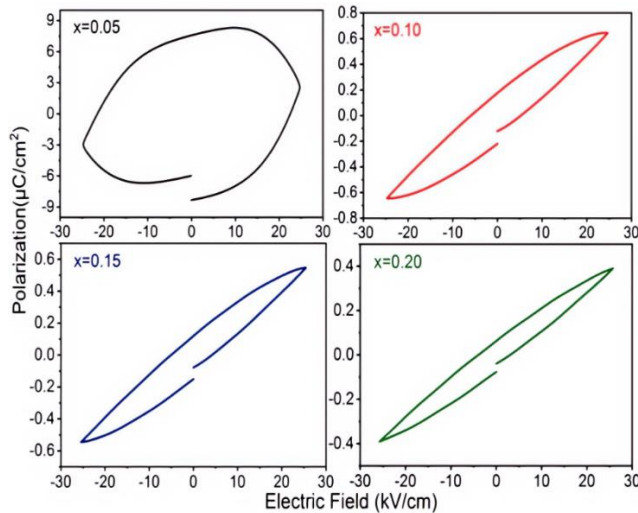


**Fig. 12** P-E hysteresis loops of  $(1-y)\text{Bi}_{1-x}\text{Nd}_x\text{FeO}_{3-y}\text{PbTiO}_3$  solid solutions with  $y=0.4$  and different  $x$  compositions.

**Table 1** Variation in Saturation polarisation ( $P_s$ ), of  $(1-y)\text{Bi}_{1-x}\text{Nd}_x\text{FeO}_{3-y}\text{PbTiO}_3$  solid solutions with the varying  $x$  and  $y$  compositions.

| Compositions<br>x | Saturation Polarisation ( $P_s$ ) $\mu\text{C}/\text{cm}^2$ |        |        |        |
|-------------------|-------------------------------------------------------------|--------|--------|--------|
|                   | y=0.1                                                       | y=0.2  | y=0.3  | y=0.4  |
| 0.05              | 2.1346                                                      | 1.9132 | 0.8296 | 2.6042 |
| 0.10              | 1.1159                                                      | 0.9993 | 0.3161 | 0.6488 |
| 0.15              | 0.8054                                                      | 0.4624 | 0.1708 | 0.5449 |
| 0.20              | 0.4351                                                      | 0.3178 | 0.1111 | 0.3923 |

**Table 2** Variation in Remnant polarisation ( $P_r$ ), of  $(1-y)\text{Bi}_{1-x}\text{Nd}_x\text{FeO}_{3-y}\text{PbTiO}_3$  solid solutions with the variation in  $x$  and  $y$  compositions.

| Compositions<br>x | Remnant Polarisation ( $P_r$ ) $\mu\text{C}/\text{cm}^2$ |        |        |        |
|-------------------|----------------------------------------------------------|--------|--------|--------|
|                   | y=0.1                                                    | y=0.2  | y=0.3  | y=0.4  |
| 0.05              | 1.0553                                                   | 0.7735 | 0.5488 | 7.9046 |
| 0.10              | 0.4792                                                   | 0.3123 | 0.0993 | 0.1909 |
| 0.15              | 0.2901                                                   | 0.0950 | 0.0787 | 0.1389 |
| 0.20              | 0.0314                                                   | 0.0059 | 0.0532 | 0.0707 |

**Table 3** Variation in Coercive Field ( $E_c$ ), of  $(1-y)\text{Bi}_{1-x}\text{Nd}_x\text{FeO}_{3-y}\text{PbTiO}_3$  solid solutions with the variation in  $x$  and  $y$  compositions.

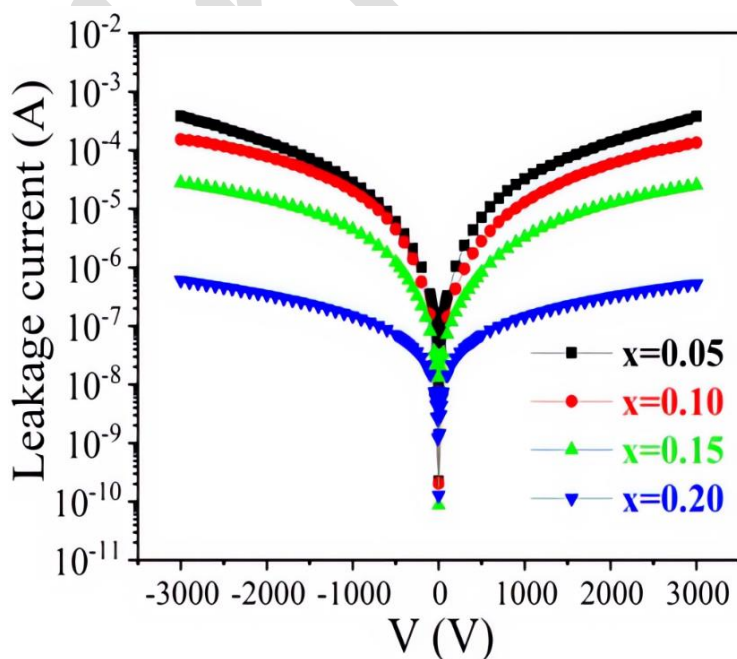
| Compositions<br>x | Coercive Field ( $E_c$ ) V/cm |        |        |         |
|-------------------|-------------------------------|--------|--------|---------|
|                   | y=0.1                         | y=0.2  | y=0.3  | y=0.4   |
| 0.05              | 8.0567                        | 6.8490 | 4.1738 | 22.0160 |
| 0.10              | 6.3756                        | 5.4957 | 2.1866 | 5.4734  |

|      |        |        |        |        |
|------|--------|--------|--------|--------|
| 0.15 | 5.6881 | 2.6572 | 2.8152 | 4.7471 |
| 0.20 | 1.3158 | 0.3358 | 2.7252 | 3.7500 |

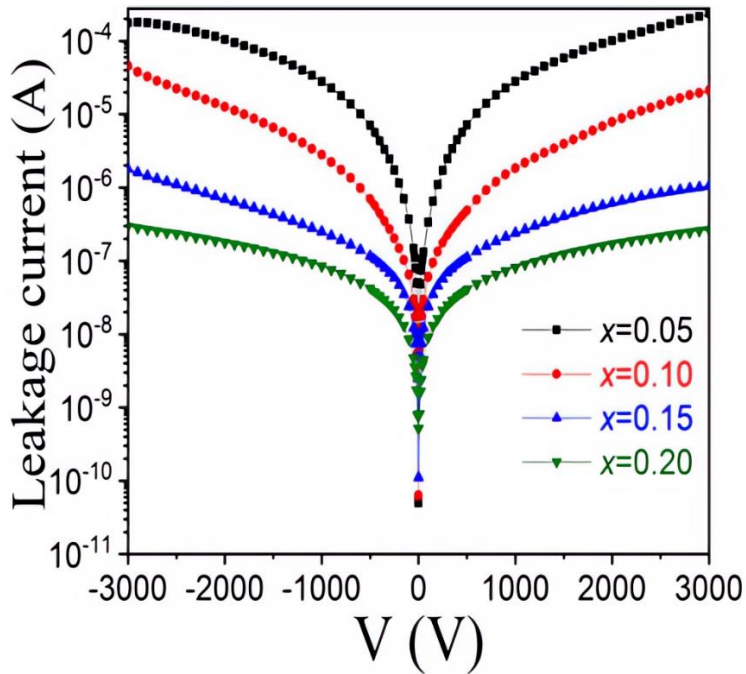
### 3.4 Leakage Current (I) vs. Voltage (V) Characteristics of Prepared Solid Solutions

Figure 13 to 16 depicts the plots between applied voltage(V) and leakage current (I) of the prepared (1-y)Bi<sub>1-x</sub>Nd<sub>x</sub>FeO<sub>3-y</sub>PbTiO<sub>3</sub> solid solutions with different x and y compositions at ambient temperature. The main drawback of the BiFeO<sub>3</sub> compound is its significant leakage current. The large leakage current has traditionally restricted the usage of BFO compounds on commercially available devices. However, substituting kinds of ions influences leakage current behaviour in different prepared samples.

The current leakage behaviour in different solid solutions is to be altered by Nd doping and found to decrease as Nd doping increases. Figures 13 to 16 show that the leakage current significantly decreases from 10<sup>-3</sup> to 10<sup>-7</sup>. For a rare-earth element doped BFO compound, Yongyuan Zang et al. obtained similar outcomes [29]. Increased Nd doping reduces charge defects brought on by oxygen vacancies and valence variations of Fe<sup>+3</sup> ions to Fe<sup>+2</sup> ions, thereby reducing leakage density. Also, since the average grain size is smaller, the grain boundary's limited conduction causes the local space charge at grain boundaries to reduce current density. [30,31].



**Fig. 13** Plots of Applied voltage(V) and leakage current (I)for  $(1-y)\text{Bi}_{1-x}\text{Nd}_x\text{FeO}_3-y\text{PbTiO}_3$ solid solutions with  $y=0.1$  and varying  $x$  compositions.



**Fig. 14** Plots of Applied voltage(V) and leakage current (I) for  $(1-y)\text{Bi}_{1-x}\text{Nd}_x\text{FeO}_3-y\text{PbTiO}_3$ solid solutions with  $y=0.2$  and varying  $x$  compositions.

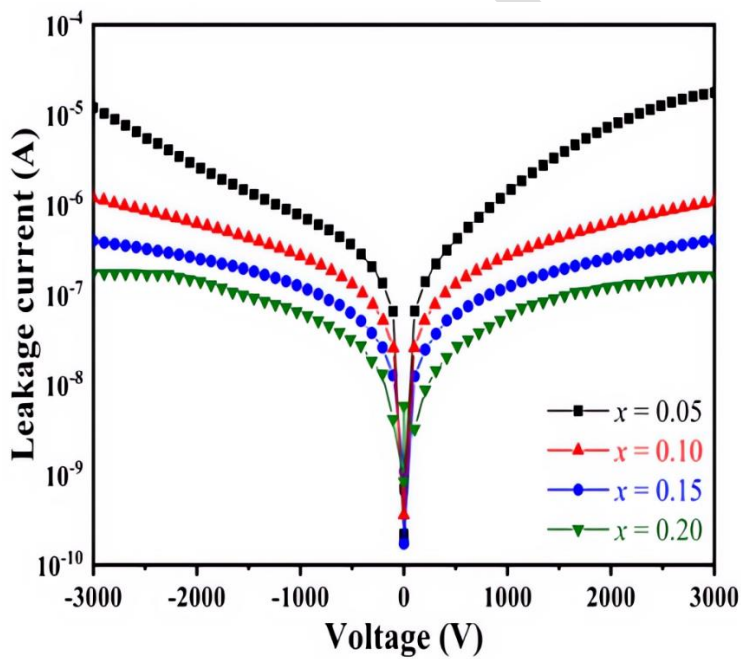


**Fig. 15** Plots of Applied voltage (V) and leakage current (I)for  $(1-y)\text{Bi}_{1-x}\text{Nd}_x\text{FeO}_3-y\text{PbTiO}_3$ solid solutions with  $y=0.3$  and varying  $x$  compositions.

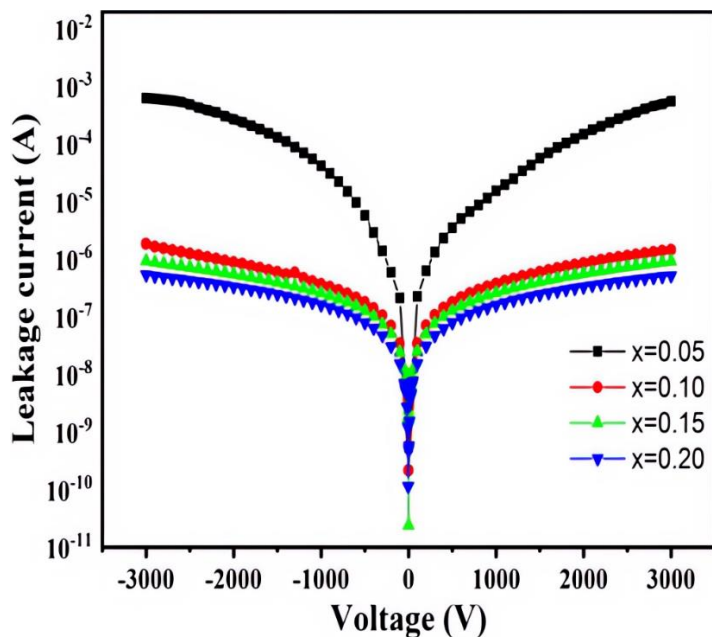


**Fig. 16** Plots of Applied voltage (V) and leakage current (I) for  $(1-y)\text{Bi}_{1-x}\text{Nd}_x\text{FeO}_{3-y}\text{PbTiO}_3$  solid solutions with  $y=0.4$  and varying compositions.

#### 4. CONCLUSIONS

We systematically investigated the electrical and ferroelectric properties of  $(1-y)\text{Bi}_{1-x}\text{Nd}_x\text{FeO}_{3-y}\text{PbTiO}_3$  solid solutions with varying  $x$  and  $y$  compositions. We have found that the dielectric constant is high at low frequencies and decreases with rising frequency, attributed to oxygen vacancies and Fe ion transitions induced by Nd doping. The dielectric loss tangent decreases with frequency for all compositions but exhibits anomalies for  $x < 0.10$  and  $y \geq 0.2$  in the 1 kHz–1 MHz range, aligning with the Debye relaxation process. The temperature-dependent dielectric permittivity suggests relaxor ferroelectric behaviour, with anomalies linked to phase transitions and multiferroic characteristics. In the ferroelectric study, saturation and remnant polarisation peak at  $x = 0.05$  Nd composition but decline with further Nd doping due to structural distortions and oxygen vacancies. For  $y > 0.3$ , polarisation increases, driven by the dominance of electric order over magnetic order. Hysteresis loops indicate a pinning effect as Nd doping rises, which may be associated with the samples' enhanced energy storage capability. Nd doping reduces leakage current by about four orders of magnitude (from  $10^{-3}$  to  $10^{-7}$ ) by



suppressing charge defects and valence variations. Grain boundary-limited conduction also contributes to reduced current density. It broadens the sample's applicability, requiring devices with stable, efficient, low-power electrical performance.

## CONFLICT OF INTEREST

The authors declare that they have no known competing financial interests or personal relationships that could have appeared to influence the work reported in this research paper.

## ACKNOWLEDGEMENT

Author Ram Chhavi Sharma is very grateful to SGT University Authority for providing research facilities during this research investigation.

## REFERENCES

- [1] Hao, X. J., "A review on the dielectric materials for high energy-storage application." *Adv. Dielectr.*, **2013**, 03, 1330001. <https://doi.org/10.1142/S2010135X13300016>.
- [2] Kumar, M. M., Srinivas, A. and Suryanarayana, S.V., "Structure-property relations in BiFeO<sub>3</sub>/BaTiO<sub>3</sub> solid solutions." *J. Appl. Phys.*, **2000**, 87, 855– 862. <https://doi.org/10.1063/1.371953>.
- [3] Malik, R.A., Hussain, A., Acosta, M., Daniels, J., Han, H.S., Kim, M.H. and Lee, J.S., "Thermal-stability of electric field-induced strain and energy storage density in Nb-doped BNKT-ST piezoceramics." *J. Eur. Ceram. Soc.*, **2018**, 38, 2511– 2519. <https://doi.org/10.1016/j.jeurceramsoc.2018.01.010>.
- [4] Cebela, M., Zagorac, D., Batalovic, K., Radakovic, J., Stojadinovic, B., Spasojevic, V. and Hercigonja, R., "BiFeO<sub>3</sub> perovskites: A multidisciplinary approach to multiferroics." *Ceram. Int.*, **2017**, 43, 1256-1264. <https://doi.org/10.1016/j.ceramint.2016.10.074>.
- [5] Baloni, M., Sharma, R.C., Singh, H., Khan, B., Singh, M.K., Sati, P.C., Thakur V.N., Kotnala, R.K. and Kumar, A., "Energy storage and Magnetoelectric coupling in neodymium(Nd) doped BiFeO<sub>3</sub>-PbTiO<sub>3</sub> solid solution." *Journal of Alloys and Compounds*, **2023**, 946, 169333. <https://doi.org/10.1016/j.jallcom.2023.169333>.

- [6] Sharma, R.C., Baloni, M. and Singh, H.,” Investigating *Magnetic and Magneto-electric Properties of Nd-doped [(1-y) Bi<sub>1-x</sub>Nd<sub>x</sub>FeO<sub>3</sub>-yPbTiO<sub>3</sub>] solid solution.*” *Journal of Magnetism and Magnetic Materials*, 2024, 595, 171916. <https://doi.org/10.1016/j.jmmm.2024.171916>.
- [7] Kumar, K.V., Voora, S. and Raghavender, A.T.,” Structural and dielectric properties of barium doped BFO.” *Mater. Today*.**2018**, 5, 26450–26459. <https://doi.org/10.1016/j.matpr.2018.08.099>.
- [8] Varshney, D. and Kumar, A.,” Structural, Raman and dielectric behaviour in Bi<sub>1-x</sub>Sr<sub>x</sub>FeO<sub>3</sub> multiferroic .” *J. Mol. Struct.*, **2013**, 1038, 242–249.<https://doi.org/10.1016/j.molstruc.2013.01.065>.
- [9] Reetu., Agarwal, A., Sanghi, S., Ashima. and Ahlawat, N.,” Structural transformation and improved dielectric and magnetic properties in Ti-substituted Bi<sub>0.8</sub>La<sub>0.2</sub>FeO<sub>3</sub> multiferroics.” *J. Phys. D: Appl. Phys.* 2012, **45**, 16500. <https://doi.org/10.1088/0022-3727/45/16/165001>.
- [10] Zia, L., Jaffari, G.H., Awan, N.A., Rahman, J. U. and Lee, S.,” Electrical response of mixed-phase (1-x) BiFeO<sub>3</sub>-xPbTiO<sub>3</sub> solid solution: Role of tetragonal phase and tetragonality.” *J. Alloys. Compd.*, **2019**,786, 98-108. <https://doi.org/10.1016/j.jallcom.2019.01.357>.
- [11] Chen, J., Xing, X. R., Liu, G.R., Li, J.H. and Liu, Y.T.,” Structure and negative thermal expansion in the PbTiO<sub>3</sub>–BiFeO<sub>3</sub> system.” *Appl. Phys. Lett.*, 2006, 89,101914.<https://doi.org/10.1063/1.2347279>.
- [12] Bhattacharjee, S. and Pandey, D.,”Stability of the various crystallographic phases of the multiferroic (1-x)BiFeO<sub>3</sub>–xPbTiO<sub>3</sub> system as a function of composition and temperature.” *J. Appl. Phys.*, **2010**,107,124112.<https://doi.org/10.1063/1.3437396>..
- [13] Khan, B., Kumar, A., Yadav, P., Singh, G., Kumar, U., Kumar, A., and Singh, M. K.,” Structural, optical, dielectric and magneto-dielectric properties of Ca<sup>2+</sup>-modified BiFeO<sub>3</sub> multiferroics.” *J. Mater. Sci.: Mater. Electron.*, **2021**,32, 18012–18027. <https://doi.org/10.1007/s10854-023-11444-0>
- [14] Yadav, P., Pandey, A., and Khan, B., Kumar, P., Kumar, A. and Singh, M. K., “Structural, optical, dielectric and magneto-dielectric properties of Ca<sup>2+</sup>-modified BiFeO<sub>3</sub> multiferroics.”

*Journal of Materials Science: Materials in Electronics*, 2023, 34(30), 2043.

<https://doi.org/10.1007/s10854-023-11444-0>.

[15] Comyn, T.P., McBride, S.P. and Bell, A.J., "Piezoelectric Properties of BiFeO<sub>3</sub>–PbTiO<sub>3</sub> ceramics." *Mat. Lett.*, **2004**, 58, 3844-3846. <https://doi.org/10.1051/jp4:2005128003>.

[16] Kumari, P., Rai, R., Sharma, S. and Valente, M. A., "Dielectric, electrical conduction and magnetic properties of multiferroic Bi<sub>0.8</sub>Tb<sub>0.1</sub>Ba<sub>0.1</sub>Fe<sub>0.9</sub>Ti<sub>0.1</sub>O<sub>3</sub> perovskite compound." *J. Adv. Dielectr.*, 2017, 7, 1750034. <https://doi.org/10.1142/S2010135X17500345>.

[17] Das, R., Kumar, P. and Choudhary, R.N.P., "Microhardness, optical and dielectric behaviour of yttria-stabilized zirconia–alumina composites." *Appl. Phys. A*, **2020**, 126, 886.

<https://doi.org/10.1007/s12648-024-03183-7>.

[18] Singh, H. and Yadav, K.L., "Synthesis and Thermal, Structural, Dielectric, Magnetic and Magnetoelectric Studies of BiFeO<sub>3</sub>-MgFe<sub>2</sub>O<sub>4</sub> Nanocomposites." *J. Am. Ceram. Soc.*, **2015**, 98, 574-579. <https://doi.org/10.1111/jace.13316>.

[19] Auromun, K., Hajra, S., Choudhary, R.N.P. and Behera, B., "Structural and electrical properties of 0.7(BiSm<sub>x</sub>Fe<sub>1-x</sub>O<sub>3</sub>)–0.3(PbTiO<sub>3</sub>) composites." *Appl. Phys. A*, 2019, 1254.

<https://doi.org/10.1007/s00339-018-2342-6>.

[20] Zang, H., Jo, W., Wang, K. and Webber, K.G., "Compositional dependence of dielectric and ferroelectric properties in BiFeO<sub>3</sub>–BaTiO<sub>3</sub> solid solutions." *Ceram. Int.*, **2014**, 40, 4759- 4765.

<https://doi.org/10.1016/j.ceramint.2013.09.020>.

[21] Kumar, S., Pal, J., Kaur, S., Sharma, V., Dahiya, S., Bahu, P.D., Singh, M., Ray, A., Maitra, T. and Singh, A., "Correlation between multiferroic properties and processing parameters in NdFeO<sub>3</sub>–PbTiO<sub>3</sub> solid solutions." *J. Alloys. Compd.*, **2018**, 764, 824–833

<https://doi.org/10.1016/j.jallcom.2018.06.058>.

[22] Sahu, T. and Behera, B., "Investigation on structural, dielectric and ferroelectric properties of samarium-substituted BiFeO<sub>3</sub>–PbTiO<sub>3</sub> composites." *J. Adv. Dielectr.*, **2017**, 7, 1750001-6.

<https://doi.org/10.1142/S2010135X17500011>.

[23] Cheng, B.L., Button, T.W., Gabby, M., Fantozzi, G. and Maglione, M.,” Oxygen vacancy relaxation and domain wall hysteresis motion in cobalt-doped barium titanate ceramics,” *J. Am. Ceram. Soc.* 2005, 88, 907-911. <https://doi.org/10.1111/j.1551-2916.2005.00167.x>.

[24] Warren, W.L., Vanheusden, K., Dimos, D., Pike, G.E. and Tuttle, B.A.,” Oxygen Vacancy Motion in Perovskite Oxides.” *J. Am. Ceram. Soc.*, **1996**, 79, 536–538.

<https://doi.org/10.1111/j.1151-2916.1996.tb08162.x>

[25] Chandrasekaran, A., Damjanovic, D., Setter, N. and Marzari, N.,” Defect ordering and defect–domain-wall interactions in PbTiO<sub>3</sub>: A first-principles study.” *Phys., Rev. B.*, 2013, 88, 214116.

<https://doi.org/10.1103/PhysRevB.88.214116>.

[26] Kumar, N., Narayan, B., Kumar, A.S., and Kumar, S.” Enhanced magneto-capacitance in Sr<sup>2+</sup> modified BiFeO<sub>3</sub>–PbTiO<sub>3</sub> solid solutions.” *Mater. Chem. Phys.*, **2020**, 252,

123313. <https://doi.org/10.1016/j.matchemphys.2020.123313> Get rights and content.

[27] Scott, J.F. and Dawber, M.,” Oxygen-vacancy ordering as a fatigue mechanism in perovskite ferroelectrics.” *Appl. Phys. Lett.*, **2000**, 76, 3801. <https://doi.org/10.1063/1.126786>.

[28] Yoon, S-J., Kang, H-W., Kucheiko, S.I., Kim, H-J., Jung, H-J., Lee, D- K. and Ahn, H.K.,” Piezoelectric properties of Pb[Zr<sub>0.45</sub>Ti<sub>0.5-x</sub>Lu<sub>x</sub>(Mn<sub>1/3</sub>Sb<sub>2/3</sub>)<sub>0.05</sub>] O<sub>3</sub> ceramics.” *J. Am. Ceram. Soc.*, **1998**,

81, 2473–2476. <https://doi.org/10.1111/j.1151-2916.1998.tb02646.x>.

[29] Zang, Y., Xie, D., Chen, Y., Li, M., Han, X., Ren, T. and Plant, D.,” Comparative Study on Structural and Ferroelectric Properties of Dual-Site Rare-Earth Ions Substituted Multi ferroelectric BiFeO<sub>3</sub>.” *Integrated Ferroelectrics. An International Journal*, 2012, 132, 30-38.

<http://dx.doi.org/10.1080/10584587.2012.660435>.

[30] Hu, H. and Krupanidhi, S.B.,” Current-Voltage characteristics of Ultrafine-grained ferroelectric Pb(Zr, Ti)O<sub>3</sub> thin films.” *J. Mater. Res.*, **1994**, 9, 1484-1498. <https://doi.org/10.1557/JMR.1994.1484>.

[31] Yang, J.K., Kim, W.S. and Park, H. H.,” Effect of grain size of Pb(Zr<sub>0.4</sub>Ti<sub>0.6</sub>)O<sub>3</sub> sol-gel derived thin films on the ferroelectric properties.” *Appl. Surf. Sci.*, **2001**, 169, 544-548.

[https://doi.org/10.1016/S0169-4332\(00\)00718-2](https://doi.org/10.1016/S0169-4332(00)00718-2).